Monthly Notices of the ROYAL ASTRONOMICAL SOCIETY

MNRAS **506,** 2232–2246 (2021) https://doi.org/10.1093/mnras/stab1279
Advance Access publication 2021 May 12

A first glimpse at the Galactic plane with the ASKAP: the SCORPIO field

G. Umana [1]★ C. Trigilio,[1] A. Ingallinera [1], S. Riggi,[1] F. Cavallaro [1,2], J. Marvil,[3] R. P. Norris [4,5], A. M. Hopkins,[6] C. S. Buemi,[1] F. Bufano,[1] P. Leto [1], S. Loru,[1] C. Bordiu [1], J. D. Bunton,[4] J. D. Collier [2,5], M. Filipovic,[5] T. M. O. Franzen,[7] M. A. Thompson [8], H. Andernach [9], E. Carretti [10], S. Dai [5], A. Kapińska,[3] B. S. Koribalski [4,5], R. Kothes,[11] D. Leahy [12], D. Mcconnell,[4] N. Tothill[5] and M. J. Michałowski [13]

[1]*INAF-Osservatorio Astrofisico di Catania, Via Santa Sofia 78, I-95123 Catania, Italy*
[2]*The Inter-University Institute for Data Intensive Astronomy (IDIA), Department of Astronomy, University of Cape Town, Private Bag X3, Rondebosch 7701, South Africa*
[3]*National Radio Astronomy Observatory, Domenici Science Operations Center 1003 Lopezville Rd, Socorro, NM 87801, USA*
[4]*CSIRO Astronomy & Space Science, P.Of. Box 76, Epping, NSW 1710, Australia*
[5]*School of Science, Western Sydney University, Locked Bag 1797, Penrith, NSW 2751, Australia*
[6]*Australian Astronomical Optics, Macquarie University, 105 Delhi Rd, North Ryde, NSW 2113, Australia*
[7]*ASTRON: The Netherlands Institute for Radio Astronomy, PO Box 2, NL-7990 AA, Dwingeloo, the Netherlands*
[8]*Centre for Astrophysics Research, Department of Physics Astronomy & Mathematics, University of Hertfordshire, College Lane, Hatfield, Herts AL10 9AB, UK*
[9]*Departamento de Astronomía, DCNE, Universidad de Guanajuato, Callejón de Jalisco s/n, Guanajuato, Mexico*
[10]*INAF, Istituto di Radioastronomia, Via Gobetti 101, Bologna, Italy*
[11]*Dominion Radio Astrophysical Observatory, Herzberg Astronomy and Astrophysics, National Research Council Canada, PO Box 248, Penticton, BC V2A 6J9, Canada*
[12]*Department of Physics and Astronomy, University of Calgary, 2500 University Dr.NW, Calgary, AB T2N 1N4, Canada*
[13]*Astronomical Observatory Institute, Faculty of Physics Adam Mickiewicz University in Poznan, ul. Sloneczna 36, PL-60-286 Poznan, Poland*

Accepted 2021 April 27. Received 2021 April 27; in original form 2021 January 19

ABSTRACT

In the broad context of the Australian Square Kilometer Array Pathfinder (ASKAP) early-science phase and preparation for the related surveys, we report the first radio observations towards the Galactic plane. The targeted field was chosen to encompass the entire SCORPIO survey, one of the several pathfinder projects for the Evolutionary Map of the Universe survey planned with the ASKAP. The observations were carried out in 2018 January at a central frequency of 912 MHz, with 15 operational antennas, and covered a total area of about 40 square degrees in three different pointings. The final image has a resolution of 24.1×21.1 arcsec^2 and a median rms of 541 μJy beam^{-1}. We were able to extract 3545 candidate sources, 75 per cent of them point sources. For a preliminary validation, a comparison with the 843 MHz Molonglo Galactic Plane Survey is presented. Although the present observations were obtained with the ASKAP only partially deployed, its unique capability to map complex sources, such as those inhabiting the Galactic plane, at different angular scales, is highlighted. Within the SCORPIO field all the previously classified H II regions, Planetary Nebulae (PNe), and supernovae remnants (SNRs), previously known to be radio sources, were detected. We also report new radio detections from several H II regions previously classified as 'candidates' or 'radio quiet' and from half of all the PNe in the SCORPIO field with robust classification. Most notably, we find numerous unclassified, extended sources which constitute a promising sample of candidates H II regions and SNRs.

Key words: techniques: image processing – techniques: interferometric – surveys – stars: evolution – stars: formation – radio continuum: general.

1 INTRODUCTION

A new era in radio astronomy has finally arrived. The Square Kilometre Array (SKA) precursors have started their early-science phase with impressive results that foreshadow their full operation. In particular the Australian SKA Array Pathfinder (ASKAP, Hotan et al. 2021) is transforming the way in which large radio surveys have been so far conducted. Due to the wide-field phased array feed (PAF) system (Chippendale, Hayman & Hay 2014) mounted on each antenna, ASKAP is capable of a huge instantaneous field of view, ∼40 square degrees, which allows the coverage of large areas of the sky in economical amounts of time (Leahy et al. 2019). The fully commissioned ASKAP has a survey speed of 220 deg^2 per hour at a target sensitivity of 100 μJy beam^{-1} at 1.4 GHz, assuming

★ E-mail: grazia.umanainaf.it

a net bandwidth of 288 MHz and a resolution of 10 arcsec.[1] The ASKAP's early-science phase started in 2016 October using 12 of the 36 antennas present in the final design. As the commissioning operations have progressed, other antennas have been added and, at the time of the reported observations, 15 antennas were operational. A number of different regions of the sky were selected for testing the array in this phase: among these, one is centred towards the same field of the 'Stellar Continuum Originating from Radio Physics in Ourgalaxy' (SCORPIO) project (Umana et al. 2015; hereafter 'Paper I'). We will refer to this targeted observation as to the 'ASKAP SCORPIO observations'.

SCORPIO is a survey of an approximately 2×2-deg^2 area of sky centred at Galactic coordinates $l = 343.5^\circ$, $b = 0.75^\circ$, conducted with the Australia Telescope Compact Array (ATCA) between 1.4 and 3.1 GHz (see Paper I for further details). Besides its own scientific goals, SCORPIO is used also as a technical test-bed for the Evolutionary Map of the Universe survey (EMU; Norris et al. 2011), an all-sky (Dec. $<$ $+30$ deg) ASKAP radio continuum sky survey scheduled to start in 2021, in particular helping to shape the strategy for its Galactic plane sections.

The Galactic plane has always been a formidable challenge for radio interferometers. A concentration of extended sources and the Galactic diffuse emission make it difficult to obtain a radio map devoid of imaging artefacts. This hampers the imaging performance of the instrument, reducing the quality of the final images (in terms of signal-to-noise ratio) and makes data reduction and analysis a particularly demanding task. Many of these issues have been mitigated by using different approaches and algorithms tuned for particular fields. However, because of the large quantity of data supplied by instruments such as the ASKAP, human intervention in every step of data reduction is infeasible and a general, though flexible, approach must be used.

In this work, we report the data reduction and analysis of the ASKAP observations of the SCORPIO field, conducted with the array still partially deployed. In Section 2, we describe the instrument set-up used and the data reduction pipeline. In Section 3, we focus on the point and extended source extraction, comparing our results to other similar surveys. Investigations of typical Galactic populations are also reported. A general discussion on the results and open problems is reported in Section 4. Finally, Section 5 summarizes this work and casts an outlook on future analysis and the ASKAP observations.

2 OBSERVATIONS AND DATA REDUCTION

2.1 The ASKAP observations

The SCORPIO field was observed with the ASKAP in band 1 (from 792 to 1032 MHz) in 2018 January using 15 antennas (of the 36 in the completed array) during the early-science phase. The array configuration had a minimum baseline of 22.4 m and a maximum baseline of 2.3 km. This implies that the observations, at the central frequency of 912 MHz, are sensitive to a minimum and maximum angular scale of 29.5 arcsec and 50 arcmin, respectively.

All the antennas were equipped with the version Mk II of the PAF specifically designed for ASKAP. Each PAF consists of 188 elements, 94 for each linear polarization. The data from each element are sent to the beamformer to create 36 independent beams, each one with a full width at half-maximum (FWHM) of 94.2 arcmin at 912 MHz. The total surveyed area covers ∼40 square degrees, which is larger by a factor 4.6 than the area covered in the previous ATCA observations (see Fig. 1). We refer to this as the ASKAP SCORPIO field in the rest of the paper.

[1] https://www.atnf.csiro.au/projects/askap/config.html

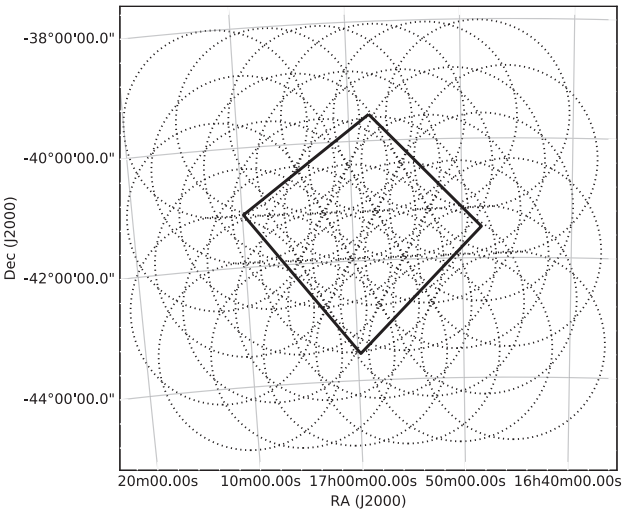

Figure 1. Comparison between the SCORPIO field coverage as observed by ATCA and by the ASKAP. The ATCA limits are represented as a solid thick line. For the ASKAP we report the position of the 36 beams (dotted circles) used for field A.

Table 1. Total observing time for each field including overheads for the bandpass and flux calibrator. The SB column reports the scheduling block ID for each data set. The observations of the field C are split in two different parts because of a hardware problem that occurred during observations.

Field	Source	SB	Time (h)
A	1934–638	5004	8
	SCORPIO	5008	
B	1934–638	5010	12
	SCORPIO	5011	
C	1934-638	5012	7
	SCORPIO	5013	
	SCORPIO	5014	4
	1934–638	5015	

The observations were carried out in the so-called 'closepack36' beam footprint (Hotan et al. 2021), consisting of three different pointings spaced by 51 arcmin with a 45-deg rotation, to optimize the sky coverage also at the highest frequency. The three pointings were conducted on three different days, and hereafter we refer to them as fields A, B, and C. The total integration time was 31 h including the observation of the standard bandpass and flux calibrator 1934–638 (see Table 1).

2.2 Data reduction

The data reduction process used the ASKAPSOFT package, based on CASACORE and specifically optimized for managing the ASKAP data (Whiting et al. 2019). The data reduction procedure is managed by a pipeline that configures and launches a series of jobs running on the Galaxy supercomputer at the Pawsey facility in Perth. As a first step data are copied from the storage location to the working area and a CASA measurement set is created for each of the 36

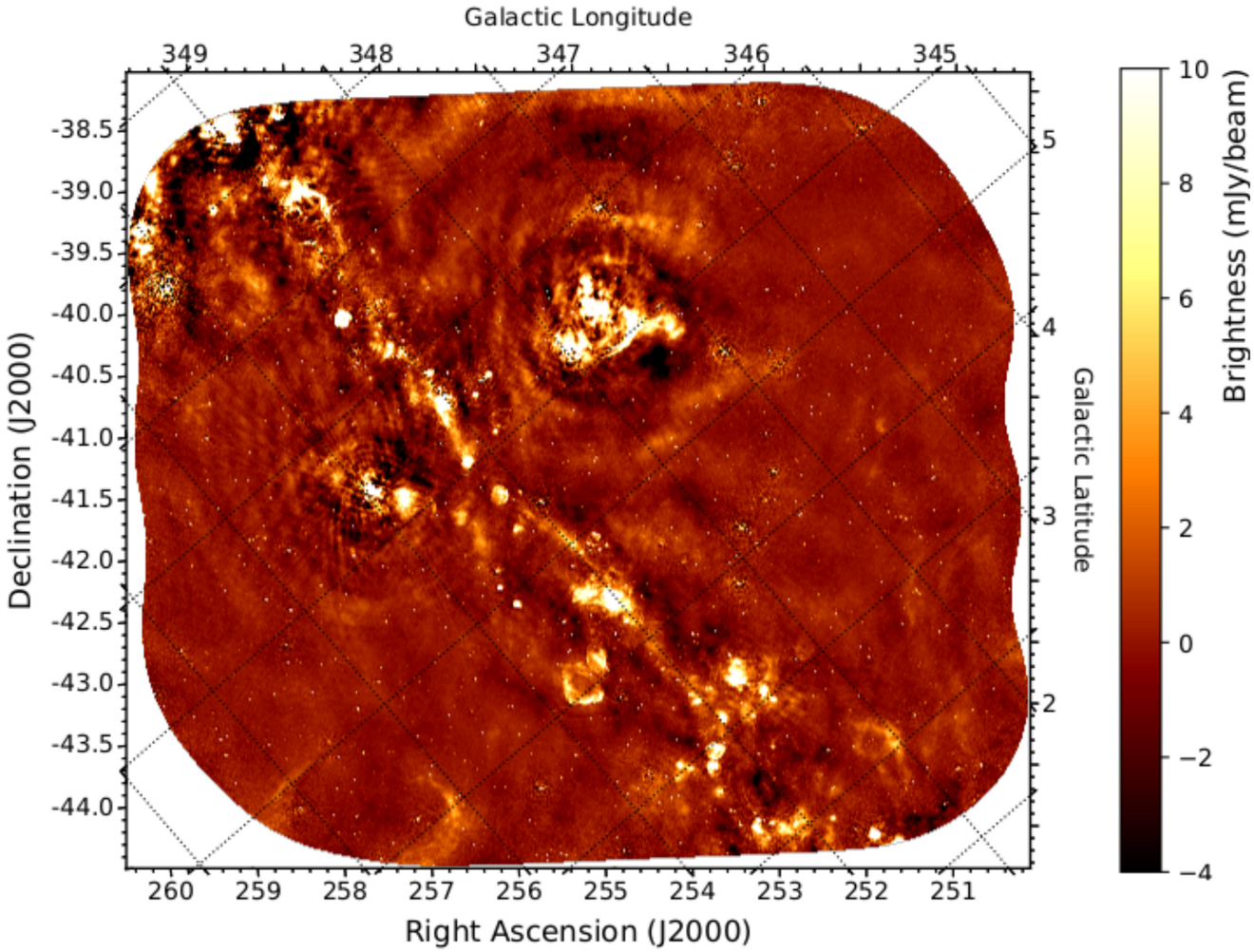

Figure 2. The ASKAP image of the SCORPIO field at 912 MHz. The mosaic covers a square region of ∼40 deg^2. The synthesized beam is 24 arcsec × 21 arcsec and the background rms noise is 150–200 μJy beam^{-1}, increasing to 500–600 μJy beam^{-1} close to the Galactic plane. The observations are sensitive to angular structures ≤50 arcmin. The silhouette of the Galactic equator is defined by a series of compact sources and bright H II regions. Several SNRs are also visible. Outside the Galactic plane some large and bright structures are evident. Among these, the region on the top centre of the field, at about 2° north from the Galactic plane, is the northern extreme of the Sco OB1 association, including the H II regions G345.45+1.50 and IC 4628. The other bright structure on the left, at about 1° south from the Galactic plane, is the H II region RCW 117.

beams. Automatic flagging is performed on bandpass calibrator and bandpass solutions are derived and applied to the target field. This, in turn, is subsequently flagged for bad data and averaged in the channel. A final flagging procedure is performed on the averaged data set. At this point, gain calibration solutions are derived. As a standard ASKAP procedure, no gain calibrator was observed during the observations (McConnell et al. 2016), because the PAF system requires an independent observation for each beam resulting in significant observing overheads. To proceed in the data reduction, a preliminary gain calibration is done using PKS 1934–638 as the calibrator, followed by several self-calibration iterations on automatically extracted bright sources present in the observed field. However this standard ASKAP reduction pipeline is best suited for extragalactic fields, where many of the brightest sources are point-like (e.g. Norris et al. 2006), and it can fail or behave in unpredictable ways for the Galactic plane where the radio sky is dominated by resolved sources and diffuse emission. To overcome this problem, we modified the standard procedure as follows. We restricted the self-calibration stage only to long baselines, selecting data with $\sqrt{u^2+v^2} \gtrsim 3344\lambda$ (corresponding to a baseline of 1100 m at 912 MHz, or angular scale $\lesssim$ 1 arcmin), a satisfactory value that we found, after attempting the data reduction with a variety of likely values. This step roughly filters out the extended emission while leaving point sources unaltered. The self-calibration is then performed and the solutions applied to all the other baselines. The self-calibration procedure is iterated three times, the first one, phase only, and then phase-amplitude self-calibration. The individual beams are finally imaged and combined together in a mosaic.

The three fields were processed separately with the final aim to merge all of them into a single map. However observations of fields B and C are affected by strong RFI and other correlator issues, as revealed from plots of the visibilities, and about 25 per cent of the data needed to be flagged.

The resulting images produced by the pipeline are therefore heavily corrupted. Manual flagging was performed on these fields to recover as much data as possible using the manual mode in the pipeline. The three fields were finally merged into a single image using a linear mosaicking procedure. The final map is shown in

Fig. 2. The synthesized beam is 24 × 21 arcsec^2 FWHM, while the background noise, calculated as the standard deviation of background pixel values, varies between ∼130 μJy beam^{-1} in regions far from the Galactic plane or other prominent extended sources and ∼2 mJy beam^{-1}, with a median value of 541 μJy beam^{-1}. The increase in background noise is mostly due to the imperfect cleaning of bright extended sources and the Galactic diffuse emission, which increases towards lower Galactic latitudes. With a maximum theoretical largest angular scale (LAS) of 50 arcmin at 912 MHz, radio structures with larger angular scales are therefore not adequately reconstructed and the image dynamic range is limited by imaging artefacts. To quantify the impact of artefacts, the residual sidelobe pattern around bright components has been measured in different regions of the ASKAP map. The obtained values vary within few per cent with position, but, in general, the artefacts due to a non-perfect cleaning determine a background noise of ∼ 0.2 per cent of the peak at a distance of 10 arcmin from the central source and, within this distance, the dynamic range is worse than 500.

3 SOURCE DETECTION

3.1 Compact source extraction and preliminary validation

The last step of the ASKAPSOFT pipeline processing is an application of the source finder algorithm SELAVY (Whiting & Humphrey 2012) to create a compact source catalogue. Default SELAVY parameters includes the selection criteria considered in the FIRST survey (Becker, White & Helfand 1995). The source finder algorithm was run on the final mosaic combining the three available fields. 3140 source islands[2] were extracted from the map with peak flux density $>5\sigma$, where σ is the local rms derived from the computed noise map. Each detected island is first processed to determine the number of blended components and finally fitted with a number of Gaussian components to estimate the integrated flux density. Among other Gaussian fitting results, SELAVY provides, for each fitted component, the peak and integrated flux densities, with their errors, the position angle, and the major and the minor FWHMs of the Gaussian component, indicating both the fit and its deconvolved value, given the image's restoring beam. After this procedure, 3545 source components are obtained for the entire field.

A continuum validation report[3] is automatically generated at the end of the pipeline processing, comparing the obtained source counts to existing measurements and models reported in the literature. The comparison is done extrapolating the ASKAP data to a frequency of 1.4 GHz, assuming a spectral index $\alpha = -0.8$ ($S \propto \nu^{\alpha}$). The result of this comparison is reported in Fig. 3. The red dots represent the differential source counts (normalized by $S^{-2.5}$) obtained with the SCORPIO ASKAP data extrapolated to 1.4 GHz. The blue dots correspond to a compilation of source counts measurements at 1.4 GHz (taken from Norris et al. 2011) fitted by a sixth-degree polynomial (dashed line).

A closer look at the plot shows that most of the SCORPIO sources are located above the fitted curve. This is again reasonable and compatible with observations towards the Galactic plane where we do expect a source excess with respect to extragalactic fields (e.g. Cavallaro et al. 2018).

[2]By 'island' we denote a group of connected pixels with fluxes above a merge threshold and around a seed pixel with flux above a detection threshold.
[3]https://confluence.csiro.au/display/askapsst/Continuum+validation + script

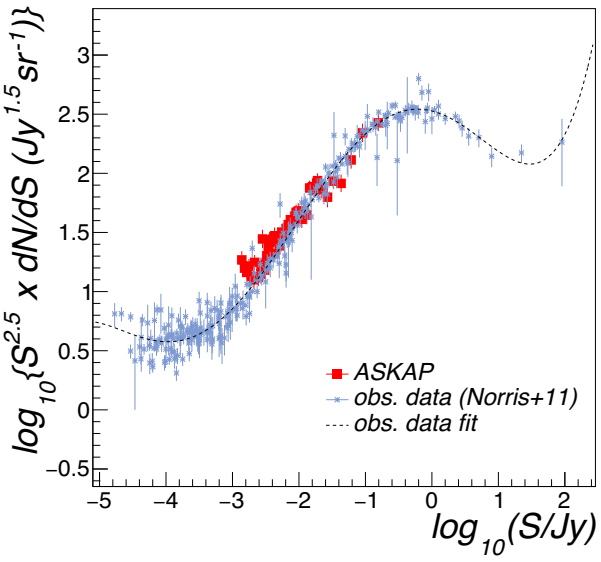

Figure 3. Differential source counts (red dots) observed with the ASKAP in the Scorpio field, normalized by $S^{-2.5}$, as a function of the source flux density S. The ASKAP fluxes were extrapolated to 1.4 GHz (assuming an average spectral index $\alpha = -0.8$) to be compared with data from Norris et al. (2011) (blue markers). The dashed line represents a sixth-degree polynomial fit of the experimental data collection.

In the companion paper (Riggi et al. 2021), the entire catalogue of the compact radio sources in the ASKAP SCORPIO field is presented. The typical performance achieved in source detection and characterization as well as the ASKAP positional and flux density scale accuracy are also discussed.

3.2 Extended sources

To perform a first visual validation of the ASKAP map, we used the second epoch Molonglo Galactic Plane Survey (MGPS-2) survey (Murphy et al. 2007), conducted with the Molonglo Observatory Synthesis Telescope (MOST). We chose MGPS-2 because it covers the entire ASKAP SCORPIO field and it is conducted at a comparable frequency (843 MHz). However, the *uv*-plane coverage is considerably different. MOST is characterized by baselines ranging from 15 to 1600 m. As a consequence, the nominal resolution is around 45 arcsec and the maximum detectable LAS is approximately twice as large as that of the ASKAP.

For extended sources the comparison is therefore not straightforward, since differences in the angular scales probed by the two instruments heavily affect the reconstructed brightness and morphology of the source. Nevertheless, some interesting considerations can be made by examining a few sample sources.

In Fig. 4, the supernova remnant SNR G343.1−0.7 imaged with the ASKAP (panel c, right) is compared to the equivalent observation made with MOST (panel a, left). To validate the ASKAP image and to check for consistency, in the central panel, (panel b), of Fig. 4, the ASKAP image of SNR G343.1−0.7, convolved to the MOST beam, ($\theta = 0.9$ arcmin), is shown. While the overall structure of the remnant is well recovered by both instruments, the ASKAP image is sharper and more sensitive, revealing additional source structure and distinguishing unrelated background point sources that are not seen with MOST. We measured the integrated flux density of the source, in the ASKAP map, through aperture photometry, applying

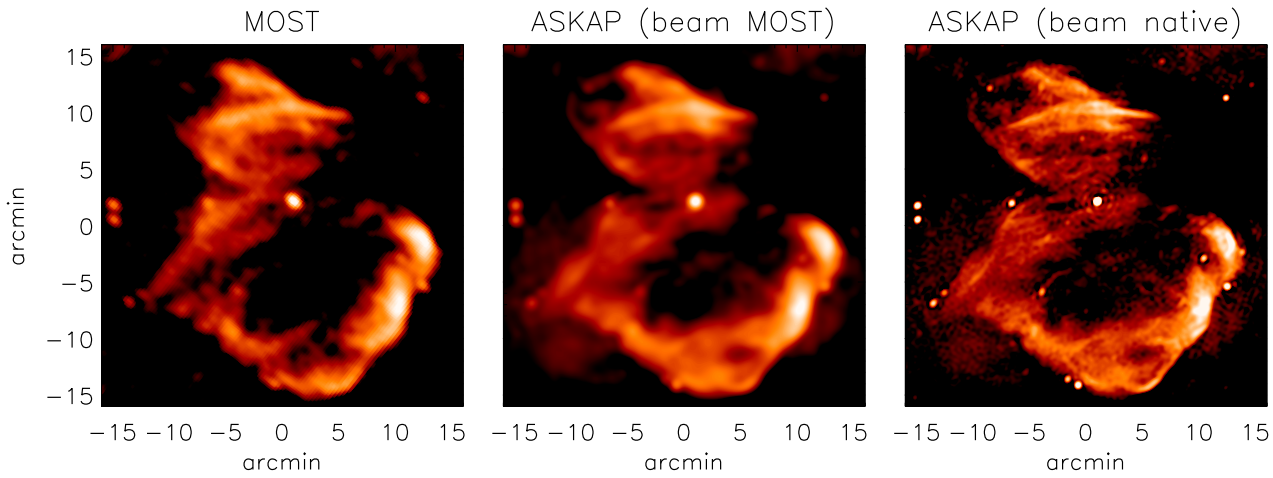

Figure 4. Images of SNR G343.1−0.7 as observed with MOST (left-hand panel) and with the ASKAP (right-hand panel). The ASKAP image of SNR G343.1−0.7, convolved to the MOST beam is shown in the central panel. The overall structure of the remnant is fully recovered by both instruments but finer details can be appreciated in the ASKAP map, where it is also possible to better distinguish sources unrelated to the remnant).

the background subtraction in a region surrounding the target, and obtained $S_{\rm int} = 7.46 \pm 0.01$ Jy, where the error associated with the integrated flux density is calculated according to $\sigma_{\rm int} = RMS \times (Nbeams)^{1/2}$, where RMS is the noise of the map, measured outside the SNR and *Nbeams* indicates the number of synthesized beams contained within the area we calculated the integrated flux density. If we, instead, measure the integrated flux density associated to the SNR but excluding the six point sources highlighted by the ASKAP (see Fig. 4, panel c), we obtain $S_{\rm int} = 7.26 \pm 0.01$ Jy. The difference in the integrated flux densities is small but significant and for other supernovae remnants (SNRs) could be more extreme. Moreover, an accurate identification of point sources that are not related to the observed SNR and whose nature is not recognized would allow a more precise analysis of the spatially resolved radio spectra to identify spectral index changes within the SNR, to be used to probe different populations of relativistic electrons that produce the observed radio emission (Egron et al. 2017). The ASKAP image shows additional details not visible in the previous MOST image. In particular, the brighter regions near the southern edges of the remnant have much greater spatial definition. These regions are potentially interacting with the local ISM and can be used to localize shocked regions.

Another illustrative example is reported in Fig. 5, where we compare the same field centred on the H II region [C06] S17 (Churchwell et al. 2006) as observed with MOST, ASKAP, and ATCA. The ATCA observations have already been presented and discussed in Paper I. Despite the great difference in terms of instrument capabilities, the overall morphology of the source is again well reconstructed by the ASKAP, which provides a good compromise between fine details and extended structures. All the compact components and detailed edges of the inner region, as detected in the ATCA image, are indeed present in the ASKAP map. Additionally, all the extended diffuse emission detected in the MOST map is also successfully recovered by the ASKAP, including the new detection of diffuse, low-brightness features in the southern part of the nebula. To compare the morphology of S17 at multiple wavelengths, we retrieved archival observations of the S17 region from Spitzer/GLIMPSE and Herschel/HiGAL. The diffuse emission recovered by the ASKAP appears to trace the ionized part of the more extended material embracing the H II region, which is also rich in both warm and cooler dust as probed by mid-IR (Spitzer) and far-IR (Herschel) observations (Fig. 6). These examples indicate the superior capability of the ASKAP, compared to other radio facilities in the Southern hemisphere, to recover fainter extended features and, at the same time, to highlight small angular scale details.

3.3 Known Galactic sources

The radio component of the Galactic plane consists of diffuse emission as well as of the contributions of discrete radio sources. Major radio surveys (Condon & Kaplan 1998; Helfand et al. 2006; Wang et al. 2018) have indicated H II regions, PNe, and SNRs as the brightest and more numerous populations of Galactic radio objects. However, the census of each of these types of object is still incomplete and has been hampered by a combination of issues, related to the capabilities of existing radio surveys, including limited frequency range, sky coverage, sensitivity, resolution, and *uv*-plane coverage.

In particular, for PNe, estimates from theoretical counts indicate that there could be up to 46 000 PNe in our Galaxy but this number could be strongly reduced to (∼6600) if it is assumed that only binary stars form a PN (Jacoby et al. 2010; Sabin et al. 2014). However, our census of PNe is largely off the expected number as the most up-to-date number of detected Galactic PNe is of only ∼3600 (Parker, Bojičić & Frew 2016). There are populations of PNe completely missed, probably those located very close to the Galactic plane, where the Hα emission, which indicates the presence of a thermal nebula, suffers from strong extinction (Ingallinera et al. 2016).

In the case of SNRs only 294 are known in our Galaxy (Green 2019), while models predict about 1000 (Tammann, Loeffler & Schroeder 1994). Existing surveys for SNRs are strongly biased towards bright and extended objects and the missing population is probably comprised of the youngest (most compact) and of lowest surface brightness SNRs.

A complete sample of PNe and SNRs will constrain their density and hence their formation rate and distribution in the Galaxy, with strong implications for models of both solar-type and massive stellar evolution.